

# Improvements in AVHRR Daytime Cloud Detection Over the ARM NSA Site

*V. Chakrapani, D. A. Spangenberg, D. R. Doelling*  
*Analytical Services & Materials, Inc.*  
*Hampton, Virginia*

*P. Minnis*  
*NASA Langley Research Center*  
*Hampton, Virginia*

*Q. Z. Trepte and R. F. Arduini*  
*Science Applications International Corporation*  
*Hampton, Virginia*

## Introduction

Clouds play an important role in the radiation budget over Arctic and Antarctic. Because of limited surface observing capabilities, it is necessary to detect clouds over large areas using satellite imagery. At low and mid-latitudes, satellite-observed visible (VIS;  $0.65 \mu\text{m}$ ) and infrared (IR;  $11 \mu\text{m}$ ) radiance data are used to derive cloud fraction, temperature, and optical depth. However, the extreme variability in the VIS surface albedo makes the detection of clouds from satellite a difficult process in polar regions. The IR data often show that the surface is nearly the same temperature or even colder than clouds, further complicating cloud detection. Also, the boundary layer can have large areas of haze, thin fog, or diamond dust that are not seen in standard satellite imagery. Other spectral radiances measured by satellite imagers provide additional information that can be used to more accurately discriminate clouds from snow and ice. Most techniques currently use a fixed reflectance or temperature threshold to decide between clouds and clear snow. Using a subjective approach, *Minnis et al. (2001)* found that the clear snow radiance signatures vary as a function of viewing and illumination conditions as well as snow condition. To routinely process satellite imagery over polar regions with an automated algorithm, it is necessary to account for this angular variability and the change in the background reflectance as snow melts, vegetation grows over land, and melt ponds form on pack ice. This paper documents the initial satellite-based cloud product over the Atmospheric Radiation Measurement (ARM) North Slope of Alaska (NSA) site at Barrow for use by the modeling community. Cloud amount and height are determined subjectively using an adaptation of the methodology of *Minnis et al. (2001)* and the radiation fields are determined following the methods of *Doelling et al. (2001)* as applied to data taken during the Surface Heat and Energy Budget of the Arctic (SHEBA). The procedures and data produced in this empirically based analysis will also facilitate the development of the automated algorithm for future processing of satellite data over the ARM NSA domain. Results are presented for May, June, and July 1998. ARM surface data are used to partially validate the results taken directly over the ARM site.

## Data

### a. AVHRR

This analysis uses all NOAA-12 (N12) and NOAA-14 (N14) Advanced Very High Resolution Radiometer (AVHRR) VIS, solar infrared (SI, 3.7  $\mu\text{m}$ ), and IR data taken over a 6° latitude by 30° longitude domain (Fig. 1) centered over the NSA site at Barrow. These data consist of High Resolution Picture Transmission (HRPT) 1-km images taken between May 1 and July 31, 1998 that encompass the ARM NSA site at Barrow. A comparison of N12 and N14 channel-3 (SI) and 4 (IR) brightness temperatures,  $T_3$  and  $T_4$ , respectively, taken during the FIRE Arctic Cloud Experiment (ACE) revealed a significant amount of image noise or striping in  $T_3$  (Minnis *et al.* 2001). To reduce the channel-3 striping, which affects cloud detection at low temperatures, a Wiener filter (Simpson and Yhann, 1994) was applied to the satellite data. Since the filter works best at low sun and at night, it was applied to only 13% of the images used in the current analysis. Figure 2 shows the improved channel-3 image after applying the Wiener filter. Although the filtered image still has some residual artifacts, it should minimize false cloud detection due to noise. Navigation corrections were applied to all N12 and N14 images before performing the cloud masking process. Clear-sky radiances were estimated for each image on a 56 X 56 km<sup>2</sup> regional grid using the method of Minnis *et al.* (2001) for the domain in Fig. 1.

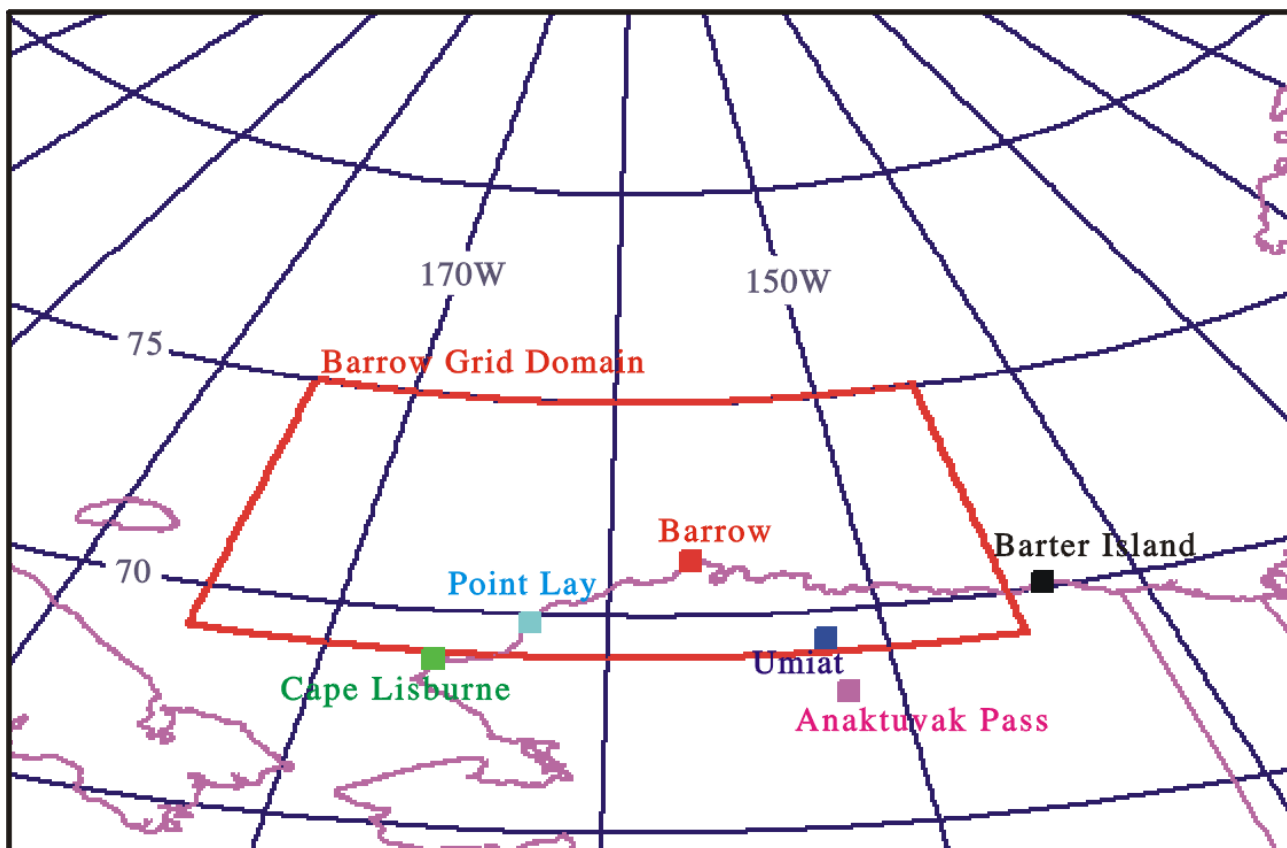


Fig. 1. NSA analysis domain.

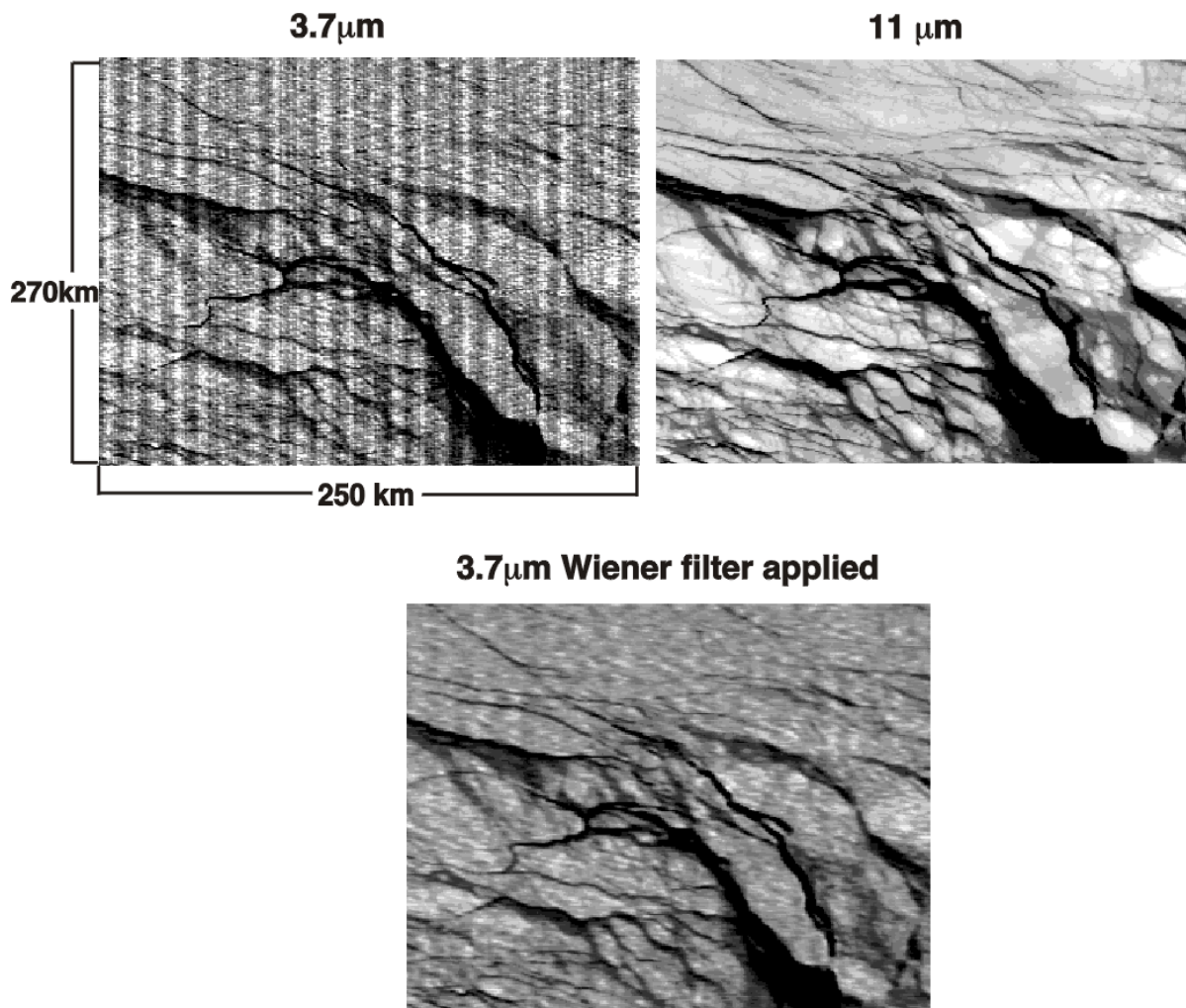


Fig. 2. Comparison of the channel 3 image before and after application of the Wiener filter.

### **b. Surface data**

Vertical profiles of temperature and humidity taken near 0000 and 1200 UTC with rawinsondes launched from the National Weather Service (NWS) at Barrow, Alaska are assumed to be representative of the entire domain. These data are used for retrievals of cloud heights and selection of the cold cloud threshold. Cloud amount in octal categories (0/8, 3/8, 5/8, 8/8) was determined every hour by the NWS Automated Surface Observing System (ASOS). These observations are compared with the AVHRR-derived cloud amounts for a 25-km radius surrounding Barrow.

## Methodology

Clouds were detected subjectively in each image by applying a visually determined brightness temperature difference  $BTD_{34}$  between channels 3 and 4 of N12 and N14. Over snow and ice surfaces,  $BTD_{34}$  is generally very small compared to its values over clouds. Clouds reflect more SI radiation from the sun that, when combined with the emitted SI radiation, yields a value of  $T_3$  that is significantly larger than  $T_4$ . For lower reflectivity surfaces like vegetated land and water,  $BTD_{34}$  is generally slightly greater or less than, respectively, the clear snow values. Thus,  $BTD_{34}$  should be a robust parameter for detecting clouds over any of those surfaces. Because the amount of reflected sunlight at  $3.7 \mu\text{m}$  varies with the viewing and illumination conditions, it is necessary to have varying thresholds for each image. These thresholds were determined for land and ocean separately for each image by carefully examining high-resolution images as in *Minnis et al. (2001)*.

Monthly mean values of  $BTD_{34}$  determined in this fashion are shown in Fig. 3 for ocean and land separately with the standard deviations. The values over land increase during July because the melting snow pack reveals more vegetation. They decrease over water because of the increasing surface temperature and the inclusion of melt ponds on the top of the ice pack (*Minnis et al. 2001*). During July 1998, the domain averaged  $BTD_{34}$  threshold values for ocean and land were 2.05 and 4.51 respectively. These threshold values were slightly increased to include haze and thin fog as clear-sky.

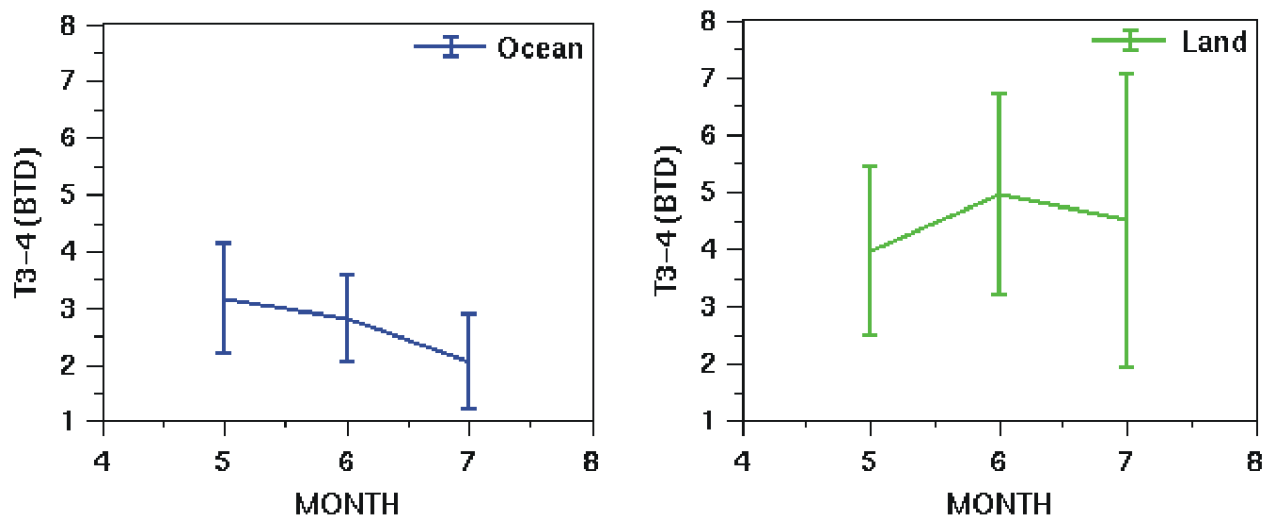


Figure 3. Monthly mean channel 3-4 brightness temperature differences.

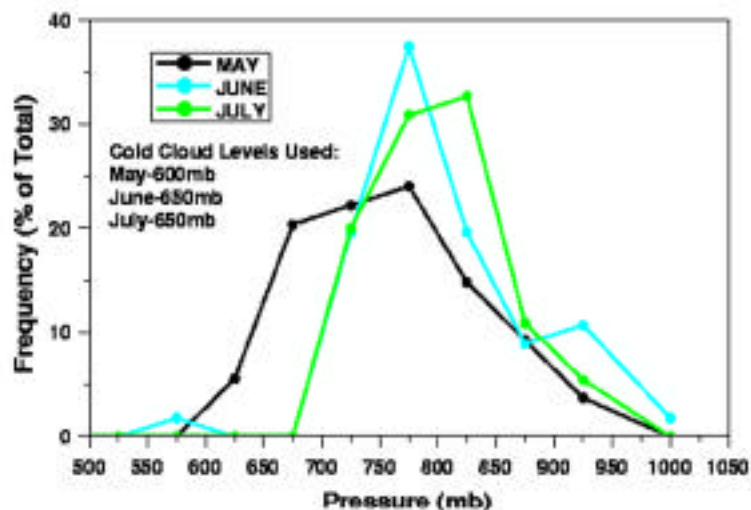


Fig. 4. Distribution of pressures with temperatures colder than lowest inversion.

The other primary cloud detection method used by *Minnis et al. (2001)* is a cold-cloud threshold. To ensure the detection of very thin cirrus clouds that may produce negligible signals in the SI data, they used the 700 hPa temperature minus 5K as the criterion to detect the cold cloud. This threshold was based on the assumption that this temperature would be warmer than the surface skin temperature during the Arctic summer. In the current analysis, the soundings for each month were examined and the cold-cloud levels were determined for each month separately. The cold-cloud threshold values are set such that they are lower than the lowest temperature on the surface-based inversions. The pressures for these threshold temperatures, plotted in Fig. 4, range from 500 to 1000 hPa. The resulting cold-cloud thresholds listed in Fig. 4 correspond to lowest pressure for each month. Thus, all three values are less than the 700 hPa values used by *Minnis et al. (2001)*.

Figure 5 shows an example of the scene classification map obtained using the *BTD34* values and the cold-cloud thresholds shown in Fig. 4. The VIS image shows a few plainly clear areas over water and land. Some of the bright areas in the VIS image are very dark in the *BTD34* image indicating the presence of snow. These areas, that are dark in the *BTD34* image and bright in the VIS image, are brighter (colder) than the clear ocean areas. The resulting image of the scene classification shows the clear water, snow, and land with the interspersed clouds. Some remaining evidence of noise in the channel-3 image is apparent in some cloud lines over the snow areas. The Wiener filter was not applied to these data because of the relatively low solar zenith angle.

In addition to deriving cloud heights  $z$ , clear SW albedo  $\alpha_{clr}$  and IR temperatures  $T_{clr}$ , total albedo  $\alpha$ , and outgoing longwave radiation *OLR*, and cloud radiative forcing were computed in the same fashion as in *Doelling et al. (2001)*. These results were averaged for each grid box and archived. Monthly and hourly means were also computed for each box using the interpolation and averaging techniques described by *Young et al. (1998)*.

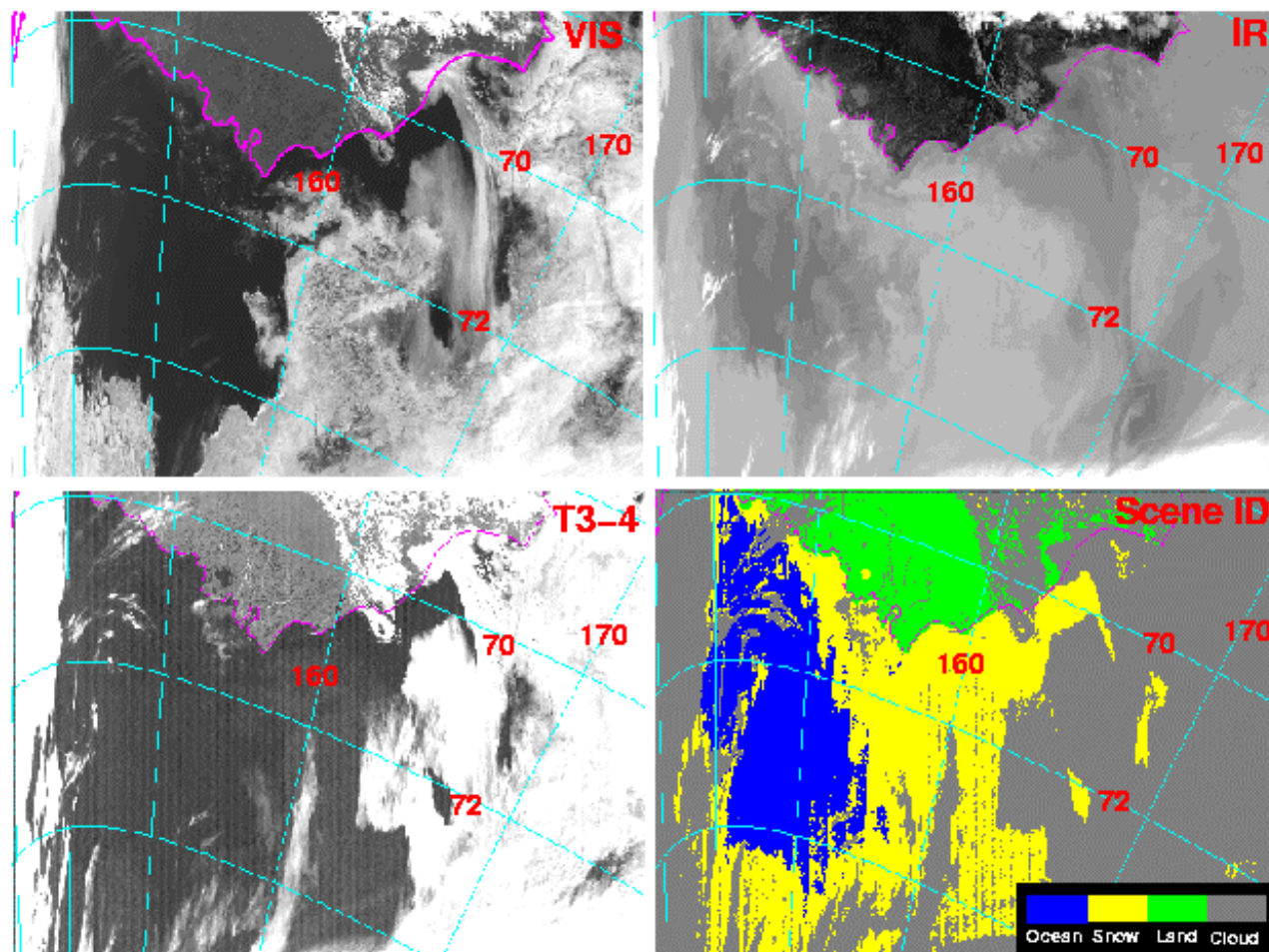


Fig. 5. NOAA-14 AVHRR and NSA scene classification for 0027 UTC, July 27, 1998.

## Results

The snows of winter still cover a significant portion of the domain during May as evinced by the clear-sky SW albedo in Fig. 6. Signs of the ice pack breakup are found along the coast west of Barrow, where  $\alpha_{clr}$  is as low as 0.35. By the end of June, the snow cover was significantly reduced over land resulting in albedos between 0.10 and 0.20. Pack ice albedos drop from a maximum of 0.78 in May to 0.58 in June to only 0.48 during July. The melting is nearly complete in the eastern and southwestern parts of the domain by the end of July. Decreasing albedos are accompanied by increased temperature gradients. The mean values of  $T_{clr}$  varied from 263 to 268 K during May and from 270 to 285 K during July.

Cloud cover also decreased during the time period. During May, the maximum mean cloud amounts were over southern part of the domain and were as great as 0.89 over a few regions (Fig.7). Cloud cover was heaviest in the western part of the domain during June and July. In the eastern part over the Arctic

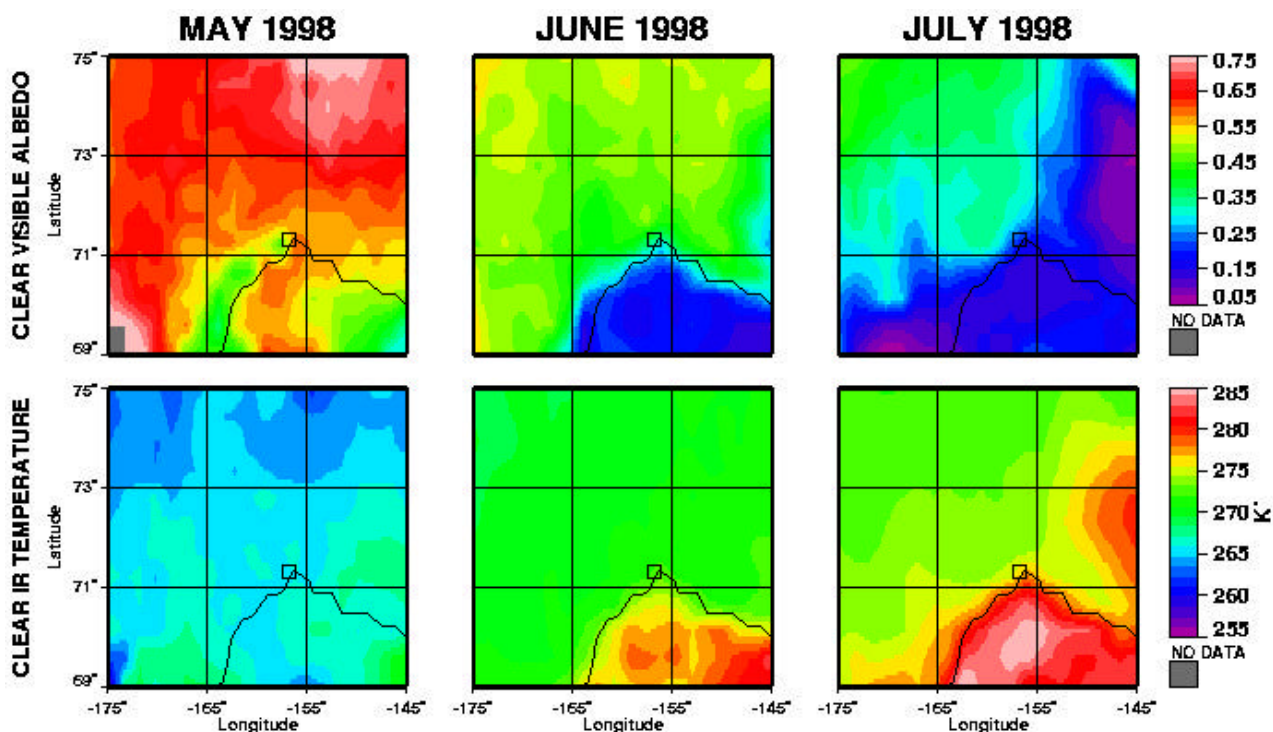


Fig. 6. Mean clear-sky radiative properties for NSA domain. Barrow is indicated with the square.

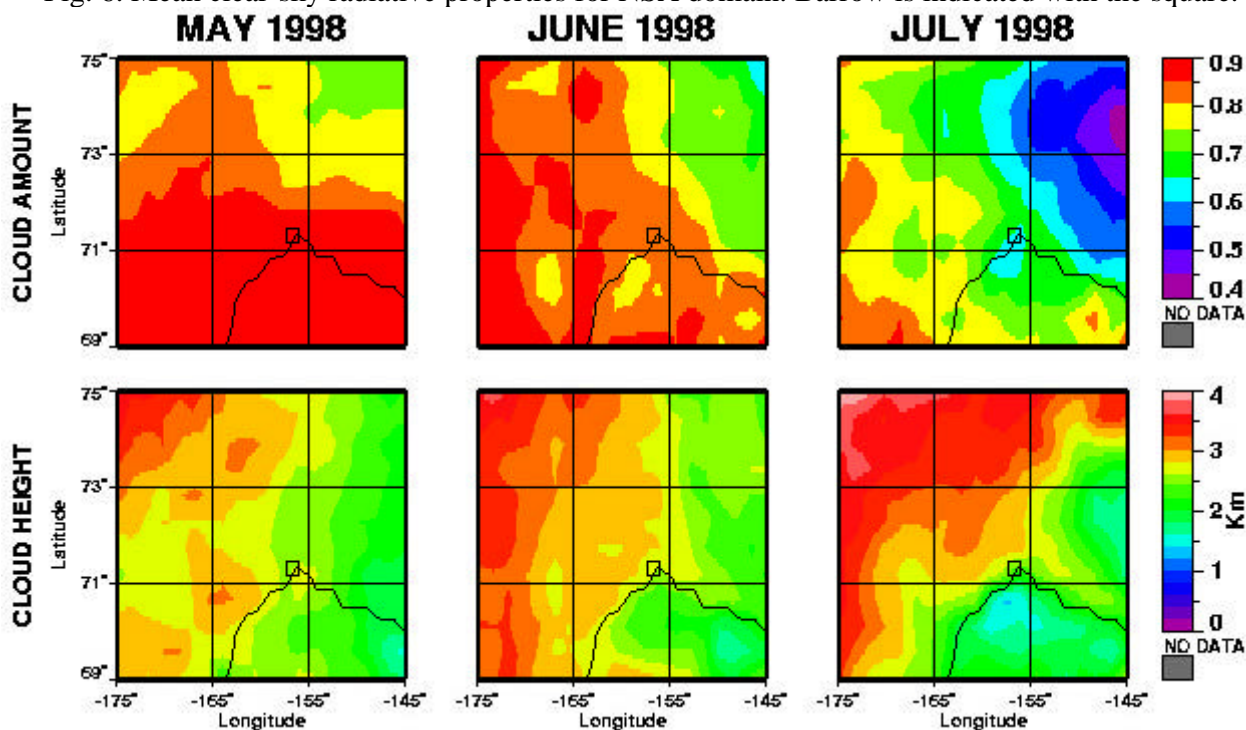


Fig. 7. Monthly mean cloud properties from AVHRR.

Ocean, the cloud amounts fell as low as 0.44 during July. Over the NSA site, the mean cloudiness ranges between 0.88 and 0.63. Cloud height is greatest in the northwest with mean values between 3.5 and 4 km during all 3 months, possibly reflecting a greater incidence of storms than the remainder of the domain. Mean cloud heights over the NSA site vary from 2 to 3 km. It appears that the values of both cloud fraction and height over Barrow are close to the average for the entire domain.

The monthly mean diurnal variations in albedo averaged over the entire domain are shown in Fig. 8 along with the mean cosine of the solar zenith angle SZA. All of the observations were taken between

0300 and 1800 LT. The albedos were interpolated using SZA-dependent directional reflectance models. The mean clear-sky albedos drop from 0.60 during May to 0.34 in July. There is little diurnal variation during May and June. During July,  $\alpha_{clr}$  varies by a factor of two during the day primarily as a result of the exposed land and ocean surfaces. Because of the heavy cloud cover, the total albedo shows a much greater diurnal variation than the clear scenes. Mean cloud amounts vary by less than 0.06, but tend to peak around 0800 LT in all cases (Fig. 9). The clear-sky OLR, or longwave LW flux, varies by only 2-3  $\text{Wm}^{-2}$  during May with a peak near local noon, but changes negligibly over the course of the day during July. This seasonal variation is similar to that seen further north over the SHEBA array (Doelling *et al.* 2001). The peak is accentuated in the total sky OLR suggesting that the clouds thin out during the afternoon exposing more of the warmer surface.

The cloud radiative forcings at the top of the atmosphere (TOA) are shown in Fig. 10. The SW cloud radiative forcing SWCRF is negative for all regions, but is close to zero over a few areas during May. The maximum (negative) values of SWCRF range from  $-70 \text{ Wm}^{-2}$  over the coast west of Barrow during

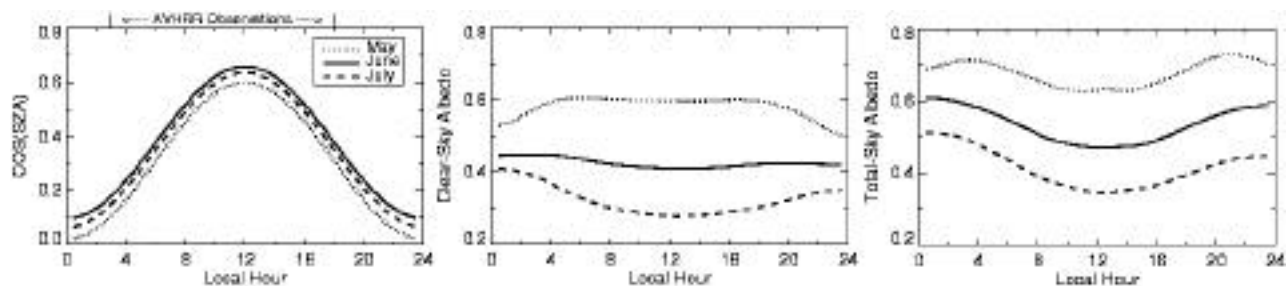


Fig. 8. Monthly mean hourly albedos over the entire NSA domain.

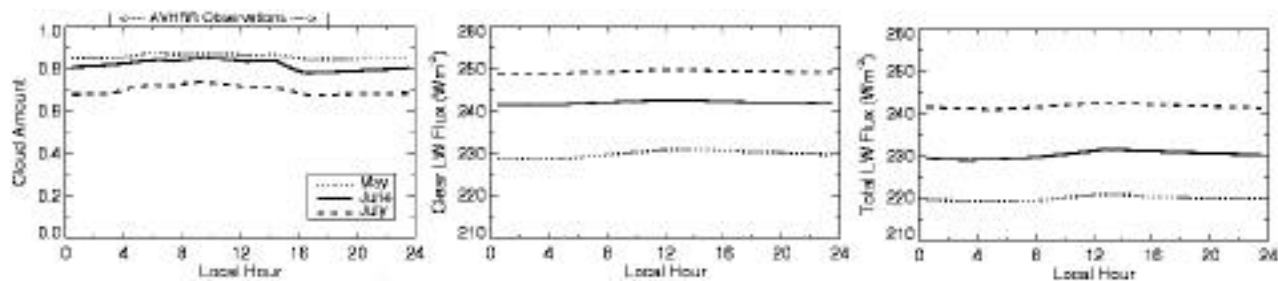


Fig. 9. Monthly mean hourly cloud amounts and OLR over the entire NSA domain.

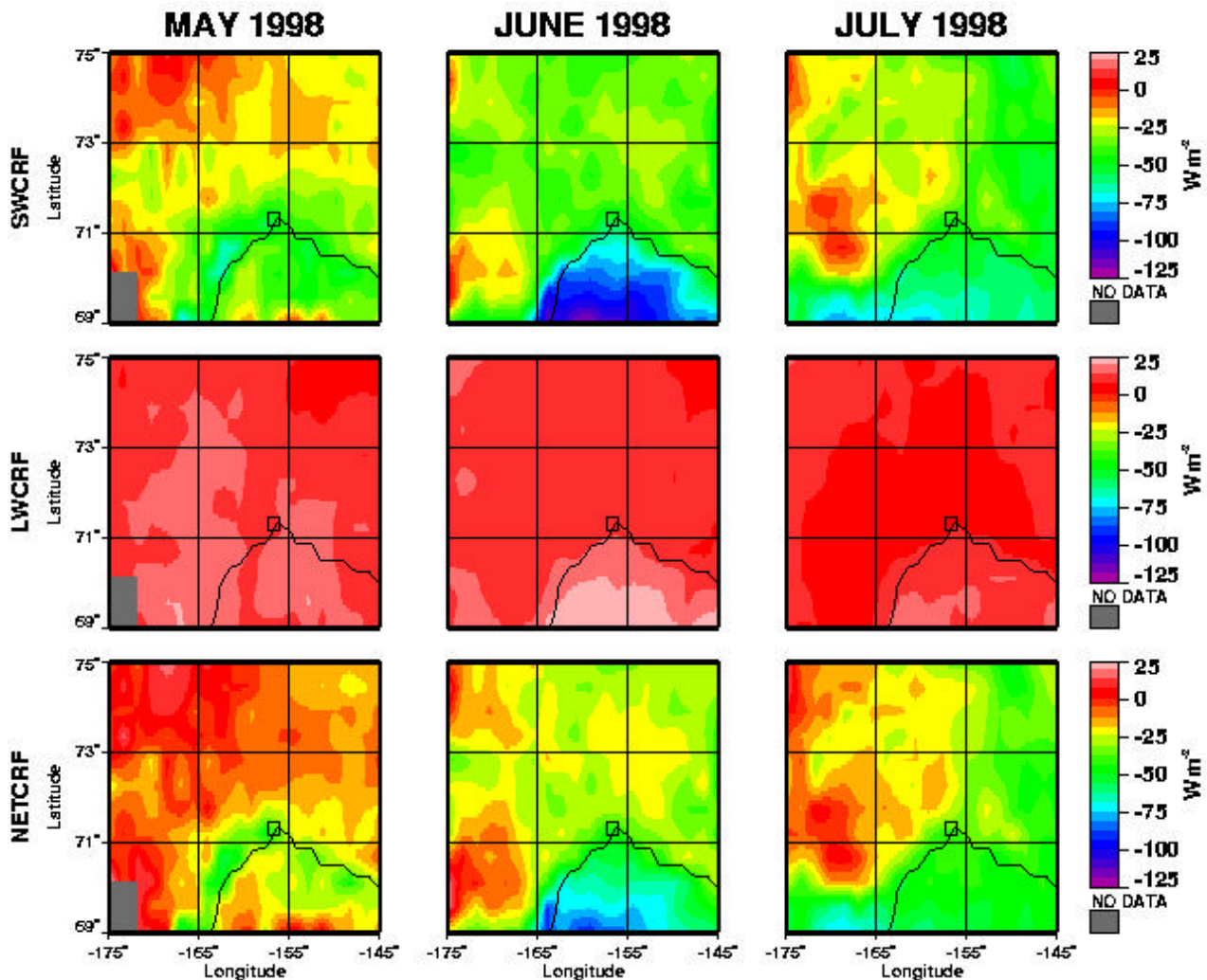


Fig. 10. Mean cloud radiative forcing over the Barrow domain.

May to  $-120 \text{ Wm}^{-2}$  over land south of Barrow during June. LW cloud radiative forcing LWCRF is less variable with a range between 2 and  $24 \text{ Wm}^{-2}$ . Over several regions in the western part of the domain, LWCRF exceeds the SWCRF resulting a positive net CRF. In general, the TOA net CRF is negative with mean values for May, June, and July of  $-12.1$ ,  $-32.5$ , and  $-30.9 \text{ Wm}^{-2}$ , respectively. This result indicates that the clouds cause a net cooling of the Earth-atmosphere system. A similar result was found over the SHEBA domain. To determine the distribution of this net CRF, it is necessary to measure the forcing at the surface.

Table 1 summarizes the comparison of the satellite and Barrow ASOS cloud amounts. The monthly mean AVHRR cloud amounts varied from 0.01 greater than to 0.04 less than the ASOS values, while the rms difference ranged from 0.15 to 0.20. These results are similar to those found over the SHEBA ship (Minnis *et al.* 2001). The large rms difference is not surprising given the coarse resolution of the ASOS results and proximity of the station to the coastline. In all cases, the mean cloud-top heights

Table 1. NWS and Barrow NSA cloud amounts.

<b>Month</b>	<b>#</b>	<b>OBS AMT</b>	<b>SAT AMT</b>	<b>BIAS</b>	<b>RMS</b>	<b>SAT TOP (km)</b>	<b>OBS BASE (km)</b>
<b>MAY</b>	73	0.906	0.892	0.014	0.145	2.4	1.5
<b>JUNE</b>	97	0.820	0.828	-0.008	0.190	2.6	2.0
<b>JULY</b>	84	0.692	0.648	0.044	0.214	2.2	1.8

Table 2. Comparison of cloud amounts in % over Barrow NSA site July 1998.

<b>BARROW</b>	<b>0-15 OBS</b>	<b>15-50 OBS</b>	<b>50-85 OBS</b>	<b>85-100 OBS</b>
<b>0-15 SAT</b>	2	7	1	0
<b>15-50 SAT</b>	5	12	6	1
<b>50-85 SAT</b>	0	6	10	11
<b>85-100 SAT</b>	0	0	5	35

exceed the cloud bases from the surface data. The results suggest that the cloud thicknesses were significantly lower during July than during the other 2 months.

Another way to summarize the cloud amount comparison is shown in Table 2. There, the July satellite cloud amounts were binned in intervals roughly corresponding to the octals reported by the ASOS. Seventy percent of the AVHRR cloud amounts are in the same range that could be represented by the ASOS results. Only two, or 2.3%, of the satellite cloud fractions differ by 2 bins. In both cases, the surface is reporting mostly cloudy or overcast while less cloudiness is seen from the satellite. No 3-bin differences occurred.

## Conclusions

The results presented here are the first retrievals of cloud fraction and height as well as radiative fluxes for the NSA domain. Based on the comparisons with National Weather Service ASOS data, the cloud amounts derived here represent well the cloudiness that occurred over the Barrow NSA domain during summer time. The determination of detailed subjective thresholds and the improvements incorporated in the current analysis are the essential factors in achieving the good agreement with surface observations. These data should be immediately useful for comparison with model estimates of cloud and radiative properties during the summer of 1998. Results from the analyses for both the SHEBA and Barrow NSA data for the time period May-July 1998 are available at the following web site: <http://www-pm.larc.nasa.gov>, hit ARM, NSA.

To minimize the labor intensive, subjective analysis of each satellite image, an automated, theoretically based cloud mask is being tested. It uses a 3.7 $\mu$ m solar reflectance threshold that depends on the viewing and illumination angles as well as the surface VIS reflectance. This threshold is determined from theoretical models of the 3.7 $\mu$ m bi-directional reflectance of snow. The information derived here and other surface observations will be used to validate the results from the automated cloud mask. Initial results using the theoretical model are promising (see *Spangenberg et al. 2001* and *Trepte et al. 2001*). The improved automated techniques will enable the processing of large volumes of AVHRR data over the ARM-NSA site continually from 1998 to the present to build long-term satellite cloud climatology over this important Arctic region. A similar approach will be used for cloud detection over the domain during night.

The cloud retrieval algorithm will be upgraded in several ways to produce accurate cloud properties. Model analysis fields will be incorporated to replace the single 2-per-day soundings over Barrow. Cloud optical depth and particle size will be retrieved although the accuracy over this domain is limited by the bright background and the lack of simultaneous measurements of 1.6 and 3.7  $\mu$ m radiances by the AVHRR (e.g., *Dong et al. 2001*). Inclusion of data from the Earth Observing System satellites Terra and Aqua could help alleviate this deficiency. In the meantime, every effort will be made to derive cloud optical depth and effective particle size using the current combination of wavelengths on the AVHRR. Comparisons with other surface observations at the NSA site, including radiometers, radar, and lidar, will be used to refine the estimates of uncertainty and improve the algorithms for analyzing the satellite data.

## Acknowledgements

This research was supported by the Environmental Sciences Division of U.S. Department of Energy Interagency Agreement DE-AI02-97ER62341 under the ARM program.

## References

- Doelling, D. R., P. Minnis, D.A. Spangenberg, C. Venkatesan, A. Mahesh, F. P. J. Valero, and S. Pope, 2001: Cloud radiative forcing during FIRE ACE derived from AVHRR data. *J. Geophys. Res.* **106**, 15,279 -15,296.
- Dong, X., G. G. Mace, P. Minnis, and D. F. Young, 2001: Arctic stratus cloud properties and their effect on the surface radiation budget; Selected cases from FIRE ACE. *J. Geophys. Res.*, **106**, 15,297 -15,312.
- Minnis, P., David R. Doelling et al., 2001: Cloud coverage and height during FIRE ACE derived from AVHRR data. *J. Geophys. Res.*, **106**, 15,215-15,232.
- Simpson, J.J., and S. R. Yhann, 1994: Reduction of noise in AVHRR channel-3 data with minimum distortion. *IEEE Trans. Geosci. Remote Sens.*, **32**, 315-328.
- Spangenberg, D. A., V. Chakrapani, D. R. Doelling, P. Minnis, and R. F. Arduini, 2001: Development of an automated Arctic cloud mask using clear-sky satellite observations taken over the SHEBA and

ARM NSA sites. *Proc. 6th Conf. Polar Meteor. and Oceanography*, San Diego, CA, May 14-18, 246-249.

Trepte, Q. Z., Arduini, R. F., Chen, Y., Sun-Mack, S., Minnis, P., Spangenberg, D. A., and D. R. Doelling, 2001: Development of a daytime polar cloud mask using theoretical models of near-infrared bidirectional reflectance for ARM and CERES. *Proc. 6th Conf. Polar Meteor. and Oceanography*, San Diego, CA, May 14-18, 242-245.

Young, D. F., P. Minnis, G. G. Gibson, D. R. Doelling, and T. Wong, 1998: Temporal interpolation methods for the Clouds and Earth's Radiant Energy System (CERES) Experiment. *J. Appl. Meteorol.*, **37**, 572-590.